CHAPTER 8

Quantitative EEG-Based Brain-Computer Interface

Bo Hong, Yijun Wang, Xiaorong Gao, and Shangkai Gao

The brain-computer interface (BCI) is a direct (nonmuscular) communication channel between the brain and the external world that makes possible the use of neural prostheses and human augmentation. BCI interprets brain signals, such as neural spikes and cortical and scalp EEGs in an online fashion. In this chapter, BCIs based on two types of oscillatory EEG, the steady-state visual evoked potential from the visual cortex and the sensorimotor rhythm from the sensorimotor cortex, are introduced. Details of their physiological bases, principles of operation, and implementation approaches are provided as well.

For both of the BCI systems, the BCI code is embedded in an oscillatory signal, either as its amplitude or its frequency. With the merits of robust signal transmission and easy signal processing, the oscillatory EEG-based BCI shows a promising perspective for real applications as can be seen in the example systems described in this chapter. Some challenging issues in real BCI application, such as subject variability in EEG signals, coadaptation in BCI operation, system calibration, effective coding and decoding schemes, robust signal processing, and feature extraction, are also discussed.

8.1 Introduction to the qEEG-Based Brain-Computer Interface

8.1.1 Quantitative EEG as a Noninvasive Link Between Brain and Computer

In the past 15 years, many research groups have explored the possibility of establishing a direct (nonmuscular) communication channel between the brain and the external world, by interpreting brain signals, such as neural spikes and cortical and scalp EEGs, in an online fashion [1–3]. This communication channel is now widely known as the brain–computer interface. BCI research originally was aimed at being the next generation of neural prostheses, to help people with disabilities, especially locked-in patients, interact with their environment. Besides potential application in clinics, BCI has been adopted as a new way of human–computer interaction as well, which can provide healthy people with an augmentative means of operating a computer when it is inconvenient for some reason to use the hands, or for computer gaming.

Basically, our brain functions—from sensation to motor control to memory and decision making—originate from microvolt-level electrical pulses, the firing (action potential) of hundreds of billions of neurons. If all or part of the neuron firings could be captured, theoretically we would be able to interpret ongoing brain activity. With the help of microelectrode arrays and computational power advancements, this kind of system has been implemented. With tens of years of exploration of motor cortex function on primates, several neurophysiology groups have been able to teach a monkey to control a computer cursor and robotic arms by using its neuron activities [4–7]. More recently, human patients have been coupled with this kind of BCI and have been able to use direct brain control to guide external devices [8]. At this level, the BCI system is dealing with the neural activity at the resolution of a single neuron, that is, at the micrometer scale. This high resolution gives neuron-based BCI a remarkable information transfer rate, which ensures real-time control of the motion trajectory of a computer cursor or a robotic arm.

Because of the invasiveness and the technical difficulty of maintaining a long-term stable recording of neuron activity, the intracranial BCI has a long way to go before it is widely accepted by paralyzed patients. This obstacle holds true for the cortical EEG-based BCI [9], which places grid and/or strip electrodes under the dura, recording local field potentials from a large population of neurons.

The electrical activity from populations of neurons not only spreads inside the dura and skull, but also propagates to the surface of the scalp, which makes it possible to conduct noninvasive recording and interpreting of neural electrical signals and, hence, possibly a noninvasive BCI [2]. However, because of volume conduction, the EEG signal captured on the scalp is a blurred version of local field potentials inside the dura. In addition, the muscle activity, eye movement, and other recording artifacts contaminate the signal more, which make it impossible to conduct a direct interpretation of such signals. As discussed in other chapters of this book, numerous efforts have been made to improve the SNR of qEEG signals. Here, in the context of BCI, the challenge of interpreting noisy qEEG signals is even harder, because a BCI system requires real-time online processing [10].

8.1.2 Components of a qEEG-Based BCI System

As shown in Figure 8.1, a qEEG-based BCI system usually consists of three essential components: (1) intent "encoding" by the human brain, (2) control command "decoding" by a computer algorithm, and (3) real-time feedback of control results. The decoding component is the kernel part of a BCI system, linking the brain and external devices. It usually consists of three steps in the process: EEG acquisition, EEG signal processing, and pattern classification.

8.1.2.1 BCI Input: Intent "Encoding" by Human Brain

In the neuron-based BCI system, the expression of subject's voluntary intent is straightforward. If the subject wants the computer cursor to move following a desired trajectory, he or she just needs to think about it as controlling his or her own hand [8]. In an EEG-based BCI system, however, there is not enough information contained in noisy EEGs for such explicit decoding and control. Typically, the con-

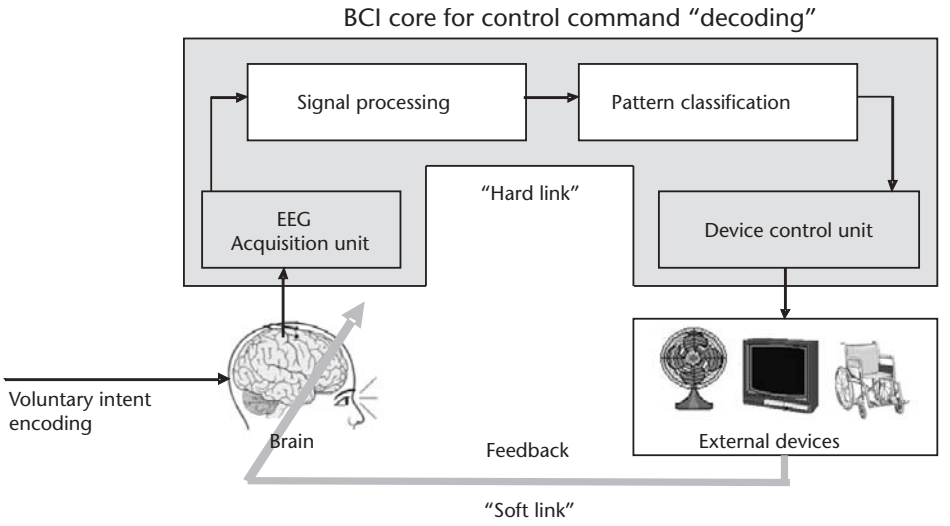

Figure 8.1 Components of BCI system.

trol command, such as moving a cursor up or down, is assigned a specific mental state beforehand. The subject needs to perform the corresponding mental task to "encode" the desired control command, either through attention shift or by voluntary regulation of his EEG [2]. Currently, several types of EEG signals exist—such as sensorimotor rhythm (SMR; also known as μ/β rhythm) [11–13], steady-state visual evoked potential (SSVEP) [14, 15], slow cortical potential (SCP) [16, 17], and P300 [18, 19]—that can be used as neural media in the qEEG-based BCI system. Among these EEG signals, SMR and SCP can be modulated by the user's voluntary intent after training, whereas the SSVEP and P300 can be modulated by the user's attention shift. In fact, the design of the EEG-based BCI paradigm is largely about how to train or instruct the BCI user to express ("encode") his or her voluntary intent efficiently [20]. The more efficient the user's brain encodes voluntary intent, the stronger the target EEG signal we may have for further decoding.

8.1.2.2 BCI Core: Control Command "Decoding" with a BCI Algorithm

Feeding the BCI system with a clear input is the function of a biological intelligent system—the brain, whereas translating input EEG signals into output control commands is the purpose of an artificial intelligent system—the BCI algorithm. Besides a high-quality EEG recording, appropriate signal processing (SP) and robust pattern classification are two major parts of a successful BCI system. Because scalp EEGs are weak and noisy, and the target EEG components are even weaker in a BCI context, various SP methods have been employed to improve the SNR and to extract meaningful features for classification in BCI [10].

Basically, these methods can be categorized into three domains: time, frequency, and space. In the time domain, for example, ensemble averaging is a widely used temporal processing technique to enhance the SNR of target EEG components, as in P300-based BCI. In the frequency domain, Fourier transform and wavelet analyses are very effective to find target frequency components, as in SMR and SSVEP-based BCI. In the space domain, spatial filter techniques such as common

spatial pattern (CSP) [21] and independent component analysis (ICA) methods [22] have been proved to be very successful in forming a more informative virtual EEG channel by combining multiple real EEG channels, as has been done for SMR-based BCI.

For most of the cases, the output of the signal processing is a set of features that can be used for further pattern classification. The task of pattern classification of a BCI system is to find a suitable classifier and to optimize it for classifying the EEG data into predefined brain states, that is, a logical value of class label. The process usually consists of two phases: offline training phase and online operating phase. The parameters of the classifier are trained offline with given training samples with class labels and then tested in the online BCI operating session. Various classifiers have been exploited in BCI research [23], among which the Fisher discriminant analysis and SVM classifiers bear the merit of robustness and better generalization ability. When considering pattern classification methods, keep in mind that the brain is an adaptive and dynamic system during interaction with computer programs. Basically, a linear classifier with low complexity is more likely to have good generalization ability and be more stable than nonlinear ones, such as a multilayer neural network.

8.1.2.3 BCI Output: Real-Time Feedback of Control Results

As shown in Figure 8.1, two links are used to interface the brain and external devices. The BCI core as described earlier comprised of a set of amplifier and computer equipment with the proper program installed can be considered as a "hard link." Meanwhile, the feedback of control results is perceived by one of the BCI user's sensory pathway, such as the visual, auditory, or tactile pathway, which serves as a "soft link" to help the user adjust the brain activity for facilitating the BCI operation.

As discussed before, the BCI user needs to produce specific brain activity to drive the BCI system. The feedback tells the user how to modify their brain's encoding in order to improve the output, as happens during a natural movement control through the normal muscular pathway. It is the feedback that closes the loop of the BCI, resulting in a stable control system. Many experimental data have shown that, without feedback, BCI performance and robustness are much lower than in the feedback case [12, 24]. From this perspective, the performance of a BCI system is not only determined by the quality of the BCI translation algorithm, but also greatly affected by the BCI user's skill of modulating his or her brain activity. Thus, a proper design for the presentation of feedback could be a crucial point that can make a difference in terms of BCI performance.

8.1.3 Oscillatory EEG as a Robust BCI Signal

Evoked potentials, early visual/auditory evoked potentials like P100 or late potentials like P300, are low-frequency components, typically in the range of tens of microvolts in amplitude. As a transient brain response, an evoked potential is usually phase locked to the onset of an external stimulus or event [25], although oscillatory EEG, such as SSVEP or SMR, has a relatively higher frequency and larger

amplitude of several hundreds of microvolts. As a steady-state response, oscillatory EEG is usually time locked to the onset of an external stimulus or internal event, without strict phase locking [25].

Some transient evoked potential-based BCIs, such as the P300 speller [18, 19], show promising performance for real application with locked-in patients [26]. However, from the perspective of signal acquisition and processing, the oscillatory EEG-based BCI has several advantages over the ERP-based BCI: (1) The oscillatory EEG has a larger amplitude and needs no dc amplification, which greatly reduce the requirement of the EEG amplifier; (2) the oscillatory EEG is much less sensitive to low-frequency noise caused by eye movement and electrode impedance change, comparing with ERP; (3) the oscillatory EEG is a sustained response and requires merely coarse timing, which allows for the flexibility of asynchronous control, whereas for ERP-based BCI, stimulus synchrony is crucial for EEG recording and analysis; and (4) with amplitude and phase information easily obtained by robust signal processing methods, such as the FFT and Hilbert transform, there are more flexible ways of analyzing oscillatory EEGs than ERPs in a single trial fashion.

For these reasons, the oscillatory EEG-based BCI will be the focus of the following two sections of this chapter. Two major oscillatory EEG-based BCIs, SSVEP and SMR-based BCI, are introduced, along with details of their physiological mechanism, system configuration, alternative approaches, and related issues.

8.2 SSVEP-Based BCI

8.2.1 Physiological Background and BCI Paradigm

Visual evoked potentials (VEPs) reflect the visual information processing along the visual pathway and primary visual cortex. VEPs corresponding to low stimulus rates or rapidly repetitive stimulations are categorized as transient VEPs (TVEPs) and steady-state VEPs (SSVEPs), respectively [27]. Ideally, a TVEP is a true transient response to a visual stimulus that does not depend on any previous trial. If the visual stimulation is repeated with intervals shorter than the duration of a TVEP, the response evoked by each stimulus will overlap each other, and thus an SSVEP is generated. The SSVEP is a response to a visual stimulus modulated at a frequency higher than 6 Hz [25]. SSVEPs can be recorded from the scalp over the visual cortex, with maximum amplitude at the occipital region (around EEG electrode Oz).

Among brain signals recorded from the scalp, VEPs may be the first kind used as a BCI control. After Vidal's pilot VEP-based BCI system in the 1970s [28] and Sutter's VEP-based word processing program with a speed of 10 to 12 words/minute in 1992 [29], Middendorf et al. [15] and Gao et al. [30] independently reported the method for using SSVEPs to determine gaze direction.

Two physiological mechanisms underlie SSVEP-based BCI. The first one is the photic driving response [25], which is characterized by an increase in amplitude at the stimulus frequency, resulting in significant fundamental and second harmonics. Therefore, it is possible to detect the stimulus frequency based on measurement of SSVEPw. The second one is the central magnification effect [25]. Large areas of the visual cortex are allocated to processing the center of our field of vision, and thus the amplitude of the SSVEP increases enormously as the stimulus is moved closer to

the central visual field. For these two reasons, different SSVEP patterns can be produced by gazing at one of a number of frequency-coded stimuli. This is the basic principle of an SSVEP-based BCI.

As shown in Figure 8.2, in a typical SSVEP-based BCI setup, 12 virtual keyboard buttons appear on a screen and flash at different frequency, while the user gazes at a button labeled with the desired number/letter. The system determines the frequency of the SSVEP over visual cortex by means of spectral analysis and looks up the predefined table to decide which number/letter the user wants to select. In the example paradigm shown in Figure 8.2, when the BCI user directs his attention or gaze at the digit button "1" flashing at 13 Hz, a 13-Hz rhythmic component will appear in the EEG signal recorded over the occipital area of scalp, and can be detected by proper spectral analysis. Thus, the predefined command "1" will be executed. Although other flashing buttons may cause interference, because of the central magnification effect, 13-Hz components are very likely to dominate the power spectrum, compared with the flashing frequencies of other buttons. In this paradigm, the rhythmic SSVEP is modulated by the BCI user's gaze direction (attention) and the conveyed information is encoded in the frequency contents of occipital EEG.

With careful optimization of the system, an average information transfer rate (ITR) of more than 40 bits per second can be achieved [30, 31], which is relatively higher than most other BCI paradigms [2]. Besides a high information transfer rate, the recognized advantages of SSVEP-based BCI include easy system configuration, little user training, and robustness of system performance. This is the reason why it has received remarkably increased attention in BCI research [14, 15, 28–35].

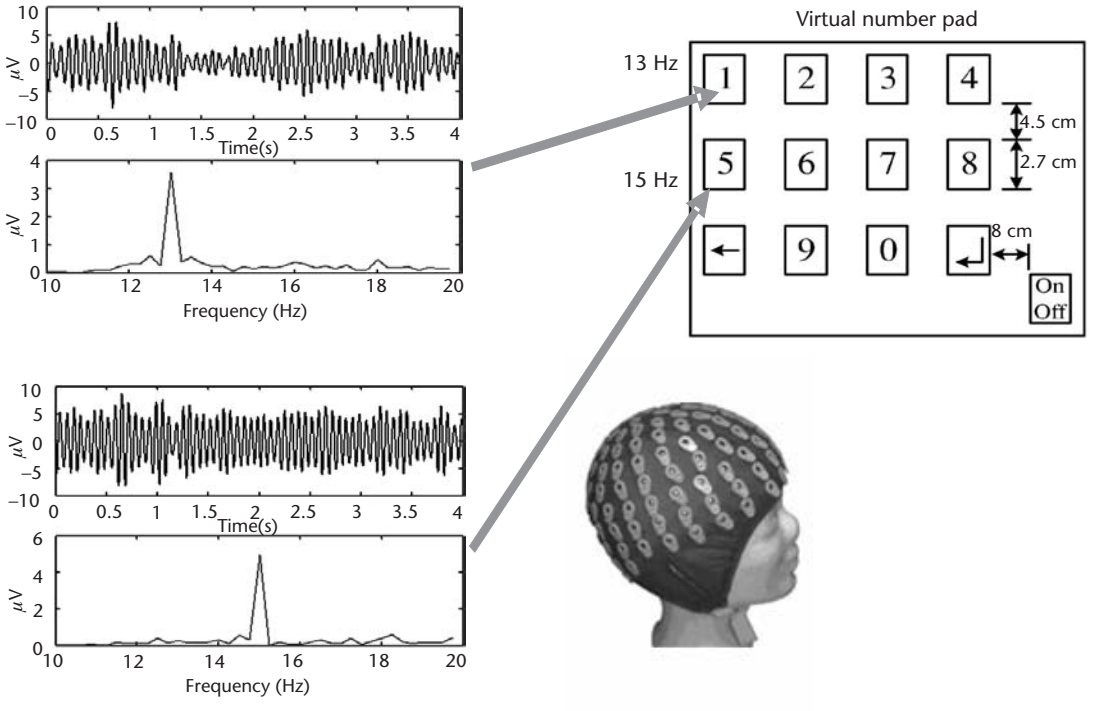

Figure 8.2 Principle of SSVEP-based BCI.

Although various studies have been done to implement and evaluate SSVEP-based BCI demonstration systems in laboratories, the challenge facing the development of a practical BCI system for real-life application is still worth emphasizing. In the following section, a practical SSVEP-based BCI system implemented in our BCI group is introduced.

8.2.2 A Practical BCI System Based on SSVEP

8.2.2.1 System Configuration

Our BCI system is composed of a visual stimulation and feedback unit (VSFU), an EEG data acquisition unit (EDAU), and a personal computer (Figure 8.3). In the VSFU, compact LED modules flickering at predefined frequency bands were employed as visual stimulators. For a typical setting, 12 LEDs in a 4-by-3 array formed an external number pad with numbers 0 through 9 and Backspace and Enter keys [Figure 8.3(b)]. When the user focused his/her visual attention on the flickering LED labeled with the number that he/she wanted to input, the EDAU and the software running on a PC identified the number by analyzing the EEG signal recorded from the user's head surface. By this means, the computer user was able to input numbers (0 through 9) and other characters with proper design of the input method. In the mode of mouse cursor control, four of the keys were assigned the UP, DOWN, LEFT, and RIGHT movements of the cursor. Real-time feedback of input characters was provided by means of a visual display and voice prompts.

Aiming at a PC peripheral device with standard interface, the hardware of a BCI system was designed and implemented as a compact box containing both an EEG data acquisition unit and a visual stimulation and feedback unit. Two USB ports are used for real-time data streaming from the EDAU and online control of the VSFU, respectively. In the EDAU, a pair of bipolar Ag/AgCl electrodes was placed over the

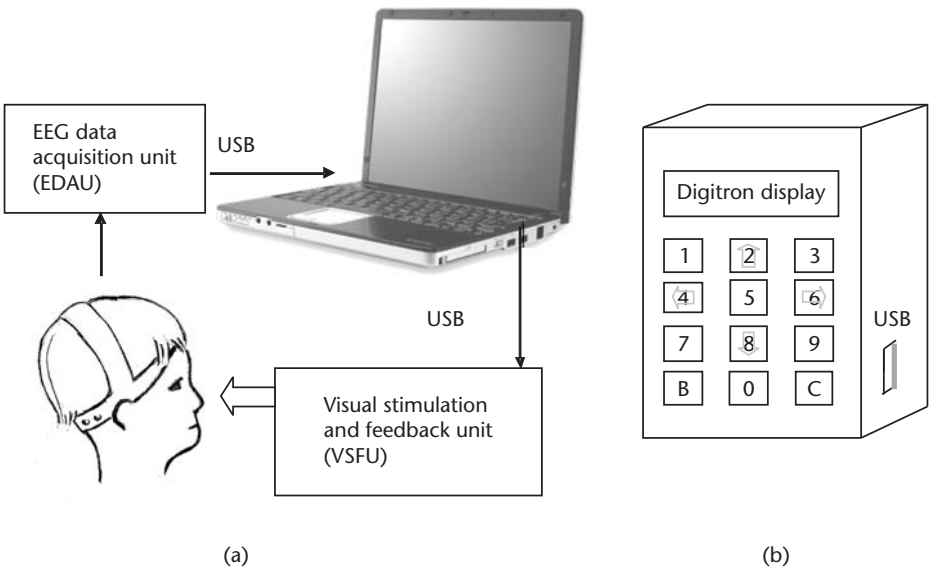

Figure 8.3 System configuration of a practical BCI using SSVEP. (a) System configuration and main components; and (b) external number pad for visual stimulation and feedback.

user's occipital region on the scalp, typically on two sites around Oz in the 10-20 EEG electrode system. A tennis headband was modified to harness the electrodes on the head surface.

The EEG signal was amplified by a customized amplifier and digitized at a sampling rate of 256 Hz. After a 50-Hz notch filtering to remove the power line interference, the digital EEG data were streamed to PC memory buffer through a USB port. For the precision of frequency control, the periodical flickering of each LED was controlled by a separate lighting module, which downloads the frequency setting from the PC through the USB port. In one of the demonstrations, our BCI system was used for dialing a phone number. In that case, a local telephone line was connected to the RJ11 port of an internal modem on the PC.

8.2.2.2 BCI Software and Algorithm

The main software running on the PC consists of key parts of the EEG translation algorithm, including signal enhancing, feature extraction, and pattern classification. The following algorithms were implemented in C/C++ and compiled into a stand-alone program. The real-time EEG data streaming was achieved by using a customized dynamic link library.

In the paradigm of SSVEP, the target LED evokes a peak in the amplitude spectrum at its flickering frequency. After a band filtering of 4 to 35 Hz, the FFT was applied on the ongoing EEG data segments to obtain the running power spectrum. If a peak value was detected over the frequency band of 4 to 35 Hz, the frequency corresponding to the peak was selected as the candidate of target frequency. To avoid a high false-positive rate, a crucial step was taken to ensure that the amplitude of a given candidate's frequency was higher than the mean power of the whole band. Herein, the ratio between the peak power and the mean power was defined as

$$Q = P_{peak} / P_{mean} \tag{8.1}$$

Basically, if the power ratio Q was higher than the predefined threshold T, then the peak power was considered to be significant. For each individual, the threshold T was estimated beforehand in the parameter customization phase. The optimal selection of the threshold balanced the speed and accuracy of the BCI system. Detailed explanation of this power spectrum threshold method can be found in previous studies [30, 31].

Due to the nonlinearity that occurs during information transfer in the visual system, strong harmonics are often found in the SSVEPs. Muller-Putz et al. investigated the impact of using SSVEP harmonics on the classification result of a four-class SSVEP-based BCI [32]. In their study, the accuracy obtained with combined harmonics (up to the third harmonic) was significantly higher than that obtained with only the first harmonic. In our experience, for some subjects, the intensity of the second harmonic may sometimes be even stronger than that of the fundamental component. Thus, analysis of the frequency band should cover at least the second harmonic, and the frequency feature has to be taken as the weighted sum of their powers, namely,

$$P(i) = \alpha P_{f1}(i) + (1-\alpha) P_{f2}(i) \quad i = 1, \ldots, N \tag{8.2}$$

where N is the number of targets and, $P_{f1}(i)$ and $P_{f2}(i)$ are, respectively, the spectrum peak values of fundamental and second harmonics of ith frequency (i.e., ith target) and α is the optimized weighting factor that varies between subjects. Its empirical value may be taken as

$$\alpha = \frac{1}{N}\sum_{i=1}^{N} P_{f1}(i) \Big/ \left(P_{f1}(i) + P_{f2}(i)\right) \tag{8.3}$$

8.2.2.3 Parameter Customization

To address the issue of individual diversity and to improve the subject applicability, a procedure of parameter customization was conducted before BCI operation. Our previous study suggests that the crucial system parameters include EEG electrode location, the visual stimulus frequency band, and the threshold (T) for target frequency determination [31]. To maintain the simplicity of operation and efficiency of parameter selection, a standard procedure was designed to help the system customization. It consists of the steps discussed next.

Step 1: Frequency Scan
Twenty-seven frequencies in the range of 6 to 19 Hz (0.5-Hz spacing) were randomly divided into three groups and the 9 frequencies in each group were randomly assigned to numbers 1 through 9 on the above-mentioned LED number pad. Then the frequency scan was conducted by presenting the numbers 1 through 9 on the digitron display one by one and each for 7 seconds. During this time period, the user was asked to gaze at the LED number pad corresponding to the presented number. This kind of scan was repeated for three sessions containing all 27 frequencies. There was a 2-second resting period between each number and a 1-minute resting period between groups. It took about 8 minutes for a complete frequency scan. The 7-second SSVEP response during each frequency stimulus was saved for the following offline analysis. In the procedure of frequency scanning, the bipolar EEG electrodes were placed at Oz (center of the occipital region) and one of its surrounding sites (3 cm apart on the left or right side). According to our previous study [31, 36], this electrode configuration was the typical one for most users.

Step 2: Simulation of Online Operation
The saved EEG segments were analyzed using the FFT to find the optimal frequency band with relatively high Q values. The suitable value of the threshold T and the weight coefficients α were estimated in a simulation of online BCI operation, in which the saved EEG data were fed into the algorithm in a stream.

Step 3: Electrode Placement Optimization
Only one bipolar lead was chosen as an input in our system. For some of the subjects, when the first two steps did not provide reasonable performance, an advanced electrode placement optimization method was employed to find the optimal bipolar electrodes. The best electrode pair for bipolar recording with the highest SNR was selected by mapping the EEG signal and noise amplitude over all possible elec-

trodes. Generally, the electrode giving the strongest SSVEP, which is generally located in the occipital region, is selected as the signal channel.

The location of the reference channel is searched under the following considerations: The amplitude of this channel's SSVEP should be lower and its position should lie in the vicinity of the signal channel such that the noise component is similar to that in the signal channel. A high SNR can then be gained when the potentials of the two electrodes are subtracted. Figure 8.4 shows an example of a significant enhancement of the SSVEP SNR derived from the lead selection method.

Most of the spontaneous background activities are eliminated after the subtraction; the SSVEP component, however, is retained. Details of this method can be found in previous studies [31, 36]. According to our observations, although the selection varies across subjects, it is relatively stable for each subject over time. This finding makes the electrode selection method feasible for practical BCI application. For a new subject, the multichannel mapping only needs to be done once to optimize the lead position.

In tests of the system based on frequency features (dialing a telephone number), with optimized system parameters for five participants, an average ITR of 46.68 bits/min was achieved.

8.2.3 Alternative Approaches and Related Issues

8.2.3.1 SSVEP Feature: Amplitude Versus Phase

In the SSVEP BCI system based on frequency coding, the flickering frequencies of the targets are not the same. To ensure sufficiently high classification accuracy, a sufficient interval should be kept between two different frequencies such that the number of targets is restricted. If phase information embedded in SSVEPs is added, the number of flickering targets may be increased and a higher ITR should be expected. An SSVEP BCI based on phase coherent detection was proposed [37], in which two stimuli with the same frequency but different phases were discriminated

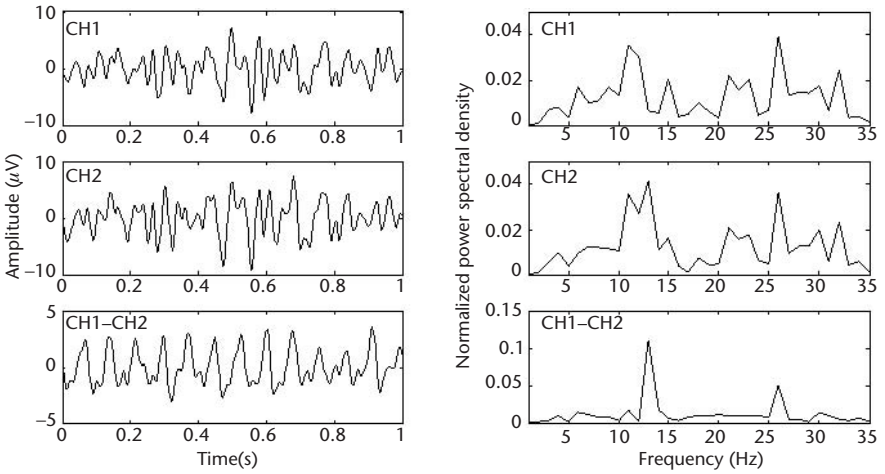

Figure 8.4 Monopolar and optimal bipolar EEGs and their normalized power spectral density of one subject. The frequency of target stimulation is 13 Hz, shown as a clear peak in the bipolar electrode derivation, along with its harmonics at 26 Hz.

successfully in their demonstration. Inspired by this work, we tried to further the work by designing a BCI system with stimulating signals of six different phases under the same frequency. Initial testing indicates the feasibility of this method.

For a phase-encoded SSVEP BCI, flickering targets on a computer screen at the same frequency with strictly constant phase difference are required. We use the relatively stable computer screen refreshing signal (60 Hz) as a basic clock, and six stable 10-Hz signals are obtained by frequency division as shown in Figure 8.5. They are used for the stimulating signal of the flickering spots on the screen to control the flashing moment of the spots. The flashing moments [shadow areas along the time axis in Figure 8.5(a)] of the spots are interlaced by one refreshing period of the screen (1/60 second). In other words, because the process repeats itself every six times, the phase difference of the flashing is strictly kept at 60 degrees (taking the flashing cycle of all the targets as 360 degrees). Six targets flickering at the same frequency with different phases are thus obtained.

During the experiment, the subject was asked to gaze at the six targets respectively. The spectrum value at the characteristic frequency (f_0=10 Hz) was calculated simply by the following formula:

$$y(f_0) = \frac{1}{N}\sum_{n=1}^{N} x(n)\exp\left[-j2\pi(f_0/f_s)n\right] \tag{8.4}$$

where f_s is the sampling frequency (1,000 Hz) and data length N is determined by the length of the time window. The complex spectrum value at 10 Hz can be displayed on a plane of complex value as shown in Figure 8.5(b). With a data length of 1 second, six phase clusters are clearly shown. The SSVEP and visual stimulus signal are stably phase locked, sharing the same phase difference of 60 degrees between targets. This makes it possible to set up several visual targets flickering under the same frequency but with different phases so as to increase the number of targets for choice. As an example, we used the system described to implement an

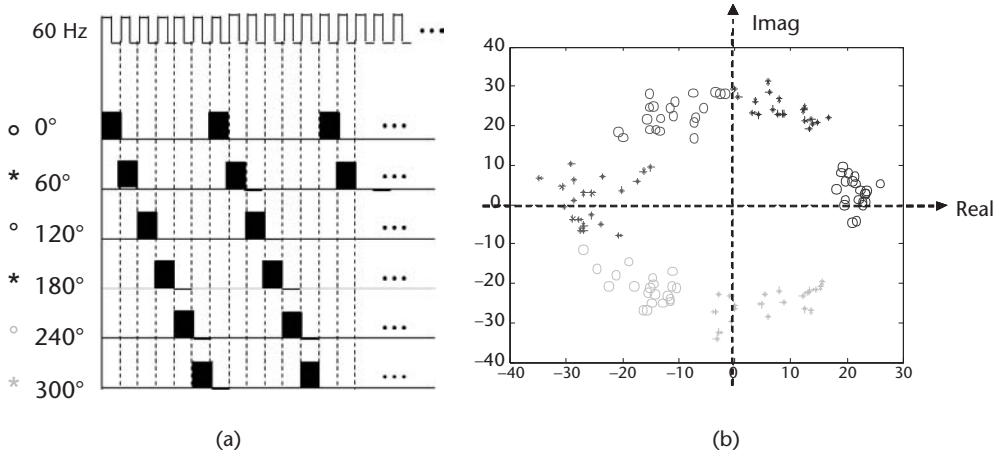

Figure 8.5 An SSVEP phase interlacing design for discrimination of multiple screen targets. (a) Timing scheme for phase interlacing of six screen targets, with shadow areas indicating the ON time of each screen target, with a reference to the cycles of CRT screen refreshing; and (b) phase clustering pattern on the complex plane indicates a discriminability among the six targets.

EEG-operated TV controller, demonstrating the practicability of phase coding in SSVEP- based BCI systems.

8.2.3.2 Coding Approach: Frequency Domain Versus Temporal Domain

According to the VEP signals used for information coding, VEP-based BCIs fall into two categories: transient VEPs and SSVEPs. The first category uses TVEPs to detect gaze direction. Spatial distributions of TVEPs elicited by a stimulus located in different visual fields were used by Vidal in the 1970s to identify visual fixation [28]. According to the approach for information coding, the SSVEP-based BCIs can be further divided into time-coded and frequency-coded subgroups. Hereafter, we refer to them as *t*SSVEP and *f*SSVEP, respectively. The BCI system described in Section 8.2.2 employs the *f*SSVEP approach. Instead of using a periodic flashing with fixed time interval between flashes, in Sutter's VEP-based BCI system, the occurrence time of visual flashes was not periodic (although it has a short interval as required by SSVEPs). The varying temporal patterns of these flashing sequences make it possible to discriminate among targets, thereby falling into the category of *t*SSVEP.

So far, both frequency decoding and temporal decoding strategies have been employed in VEP-based BCI research. Feature extraction of the TVEP is based on waveform detection in the temporal domain [38, 39]. Similarly, a template matching approach by cross-correlation analysis was used to detect the *t*SSVEP in the BRI system [29]. For a frequency-coded design, the amplitude of the *f*SSVEP from multiple flashing targets is modulated by gaze or spatial attention, and detected by using power spectral density estimation. Note that analysis of the TVEP and *t*SSVEP methods needs accurate time triggers from the stimulator, which can be omitted in frequency amplitude-based detection of the SSVEP.

8.2.3.3 Muscular Dependence: Dependent Versus Independent BCI

According to the necessity of employing the brain's normal output pathways to generate brain activity, BCIs are divided into two classes: dependent and independent [2, 40]. The VEP system based on gaze detection falls into the dependent class. The generation of the desired VEP depends on gaze direction controlled by the motor activity of extraocular muscles. Therefore, this BCI is inapplicable for people with severe neuromuscular disabilities who may lack reliable extraocular muscle control.

Totally different from amplitude modulation by gaze control, recent studies on visual attention also reveal that the VEP is modulated by spatial attention and feature-based attention independent of neuromuscular function [41, 42]. These findings make it possible to implement an independent BCI based on attentional modulation of VEP amplitude. Only a few independent SSVEP-based BCIs have been reported, in which the amplitude of SSVEPs elicited by two flashing stimuli were covertly modulated by the subject's visual attention, without shifting gaze [34, 40, 43]. Compared with the dependent type, this attention-based BCI needs more subject training, attention, and concentration. The amplitude of SSVEP elicited by attention shifting is much lower than that elicited by gaze shifting, which poses a challenge when pursuing a high information transfer rate [34, 40].

8.2.3.4 Stimulator: CRT Versus LED

In an SSVEP-based BCI, the visual stimulator serves as a visual response modulator and a virtual control panel, thus it is a crucial aspect of system design. The visual stimulator commonly consists of flickering targets in the form of color alternating or checkerboard reversing. Usually, the CRT/LCD monitor or flashtube/LED is used for stimulus display. A computer monitor is convenient for target alignment and feedback presentation by programming. But for a frequency-coded system, the number of targets is limited due to the refresh rate of the monitor and poor timing accuracy of the computer operating system. Therefore, an LED stimulator is preferable for a multiple-target system. The flickering frequency of each LED can be controlled independently by a programmable logic device. Using such a stimulator, a 48-target BCI was reported in [30].

The number of stimulation targets can be up to 64, leading to various system performances. Generally, the system with more targets can achieve a higher information transfer rate. For example, in tests of a 13-target system, the subjects had an average information transfer rate of 43 bits/min [31]. However, due to the fact that a stimulator with more targets is also more exhausting for users, the number of targets should be considered by evaluating the trade-off between system performance and user comfort.

8.2.3.5 Optimization of Electrode Layout: Bipolar Versus Multielectrode

As we know, using a small number of electrodes can reduce the cost of hardware while improving the convenience of system operation. The Oz, O1, and O2 electrode positions of the international 10-20 system are widely used in SSVEP-based BCI. As shown in Section 8.2.2.3, in our system, we use a subject-specific electrode placement method to achieve a high SNR for the SSVEPs, especially for the subjects with strong background brain activities over the area of the visual cortex [31, 36].

In the near future, more convenient electrode designs, for example, the dry electrode [44], will be highly desirable as replacements for the currently used wet electrode. Under this circumstance, it is acceptable to use more electrodes to acquire more sufficient data to fulfill detection of SSVEP signals with multichannel data analysis approaches, for example, spatial filtering techniques described in [45] and the canonical correlation analysis method presented in [46]. An additional advantage of multiple-channel recording is that no calibration for electrode selection is needed.

8.3 Sensorimotor Rhythm-Based BCI

8.3.1 Physiological Background and BCI Paradigm

In scalp EEGs, the occipital alpha rhythm (8 to 13 Hz) is a prominent feature especially when the subject is in the resting wakeful state. This kind of spontaneous alpha rhythm is usually called “idling” activity. Besides visual alpha rhythm, a distinct alpha-band rhythm, in some circumstance with a beta-band accompaniment (around 20 Hz), can be measured over the sensorimotor cortex, which is called sensorimotor rhythm (SMR) [47, 48]. The mu and beta rhythms are commonly con-

sidered as EEG indicators of motor cortex and adjacent somatosensory cortex functions [49]. When the subject is performing a limb movement, thinking about a limb movement, or receiving a tactile/electrical stimulation on a limb, a prominent attenuation of ongoing mu rhythm can be observed over the rolandic area on the contralateral hemisphere [47, 48].

Following Pfurtscheller's classical work in the 1970s [50], this SMR attenuation is usually termed event-related desynchronization (ERD), whereas the increases in SMR amplitude are termed event-related synchronization (ERS). Moreover, the spatial distribution of ERD/ERS is closely related to the body map on the sensorimotor cortex. For example, the left hand and right hand produce the most prominent ERD/ERS pattern in the corresponding hand area in the contralateral sensorimotor cortex (Figure 8.6).

Thinking about, or imagining, a limb movement generates SMR patterns that are similar to those generated during real movement. These real/imagined movement patterns make up the physiological basis for SMR-based BCI (in some of the literature, this is also termed motor imagery-based BCI, or mu rhythm-based BCI) [13, 47, 48, 51].

In recent years, BCI systems based on classifying single-trial EEGs during motor imagery have developed rapidly. Most of the current SMR-based BCIs are based on characteristic ERD/ERS spatial distributions corresponding to different motor imagery states, such as left-hand, right-hand, or foot movement imagination. The first motor imagery-based BCI was developed by Pfurtscheller et al. and was based on the detection of EEG power changes caused by ERD/ERS of mu and beta rhythms during imagination of left- and right-hand movements [47]. As shown in Figure 8.6, for example, imagination of left-hand movement causes a localized decrease of

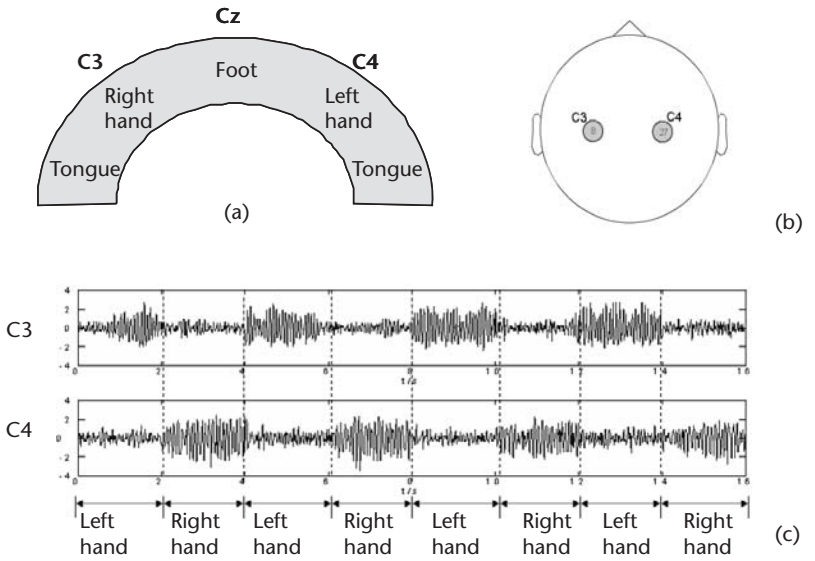

Figure 8.6 Basic principle of SMR-based BCI. (a) Approximate representation areas of body parts shown in the coronal section of the sensorimotor cortex; (b) position of C3/C4 electrode on the scalp; and (c) typical EEG (bandpass filtered at 4 to 30 Hz, covering the mu and beta bands) during imagination of left- or right-hand movement, which shows a distinct temporal pattern on the C3/C4 electrode.

mu-band power around electrode C4 (over the corresponding cortex area of the left hand). Accordingly, right-hand imagery causes a similar mu-band power decrease on electrode C3. This makes it possible for a classifier to discriminate the states of left- or right-hand motor imagery just by using spatial distribution of mu-band power.

Another SMR-based BCI approach proposed by Wolpaw et al. was to train the users to regulate the amplitude of mu and/or beta rhythms to realize two-dimensional control of cursor movement [12]. Two linear equations were used to transform the sum and the difference of EEG power over left and right motor areas into vertical and horizontal movement of screen cursors.

8.3.2 Spatial Filter for SMR Feature Enhancing

In SMR-based BCI, localized spatial distribution of SMR is a crucial feature other than its temporal power change. Because EEG has very poor spatial resolution due to volume conduction, constructing virtual EEG channels using a weighted combination of original EEG recordings is a commonly used technique to get a clear local EEG activity, or "source activity" [21, 52]. The general idea of spatial filtering can be denoted by the following equation:

$$\mathbf{Y} = \mathbf{F} \cdot \mathbf{X} \tag{8.5}$$

where **X** is the original EEG data matrix, containing recordings from each electrode in its rows; and **F** is a square transformation matrix to project the original recordings to virtual channels in the new data matrix **Y**. Each row in **Y**, as a virtual channel, is a weighted combination of all (or part of) the original recordings. The filtered data matrix **Y** is supposed to be better than **X**, for extraction of task-related features.

So far, for SMR signal enhancement, two categories of spatial filters have been explored. One category is based on EEG electrode placement, such as common average reference (CAR) and Laplacian methods [53]. CAR virtual channels are obtained by subtracting the average signal across all EEG electrodes from each original channel, as shown in the following formula of weighted combination:

$$V_i^{CAR} = V_i^{ER} - \frac{1}{n}\sum_{j=1}^{n} V_j^{\mathrm{ER}} \quad i = 1, \ldots, n \tag{8.6}$$

where n is the number of electrodes and V_i^{ER} is the original EEG recording. Similarly, the Laplacian channels are constructed by removing contributions of neighboring electrodes from the central electrode as follows:

$$\begin{aligned} V_i^{\mathrm{LAP}} &= V_i^{\mathrm{ER}} - \sum_{j \in S_i} g_{ij} V_j^{\mathrm{ER}} \\ g_{ij} &= \left(1/d_{ij}\right) \Big/ \sum_{k \in S_i} \left(1/d_{ik}\right) \end{aligned} \tag{8.7}$$

where S_i is a subset of neighboring electrodes of the ith electrode and d_{ij} denotes the geometric distance between electrode i and electrode j. If S_i consists of the near-

est-neighbor electrodes, the method is called small Laplacian. If the elements in S_i are the next-nearest-neighbor electrodes, which have a larger distance to the central electrode, it is called large Laplacian. Both CAR and Laplacian methods serve as a spatial highpass filter, which enhances the local activity beneath the current electrodes. A comparison between these spatial filter shows that both the CAR and large Laplacian methods provide a better extraction of mu rhythm in SMR-based BCI [2, 53] than the small Laplacian method. This implies that although the SMR activity is a local one, it has a fairly broad spread.

The other category is the data-driven subject-specific spatial filter, which includes PCA, ICA, and common spatial pattern (CSP). Among these three filters, the PCA and ICA spatial filters are obtained through unsupervised learning, under certain statistic assumptions. Although they have been employed in some EEG-based BCI studies [22], manual intervention of the component selection is always a problem. Up to now, the CSP method is considered to be the most effective spatial filtering technique for enhancing SMR activity, and it has been successfully applied in many BCI studies [21, 52, 54].

Similar to the spatial filtering function described in (8.5), the main idea of CSP is to use a linear transform to project the multichannel EEG data into low-dimensional spatial subspace with a projection matrix, each row of which consists of the weights corresponding to each channel. This transformation can maximize the variance of two-class signal matrices. The EEG signals under two tasks A and B can be modeled as the combination of task-related components specific to each task and nontask components common to both tasks. In the case of discrimination of left- and right-hand imagery through EEGs, the aim of the CSP method is to design two spatial filters ($\mathbf{F}_L$ and $\mathbf{F}_R$), which led to the estimations of task-related source activities ($\mathbf{Y}_L$ and $\mathbf{Y}_R$) corresponding to left hand and right hand, respectively. Then, spatial filtering is performed to eliminate the common components and extract the task-related components. The $\mathbf{Y}_L$ and $\mathbf{Y}_R$ terms are estimated by $\mathbf{Y}_L = \mathbf{F}_L \cdot \mathbf{X}$ and $\mathbf{Y}_R = \mathbf{F}_R \cdot \mathbf{X}$, where $\mathbf{X}$ is the data matrix of preprocessed multichannel EEGs.

The calculation of the spatial filter matrix $\mathbf{F}_L$ and $\mathbf{F}_R$ is based on the simultaneous diagonalization of the covariance matrices of both classes. The EEG data of each trial is first bandpass filtered in the desired mu or beta band and then used to form matrix $\mathbf{X}_L$ and $\mathbf{X}_R$ of size $N * M$, where N is the number of EEG channels and M is the data samples for each channel. The normalized spatial covariance can be calculated as

$$\mathbf{R}_L = \frac{\mathbf{X}_L \mathbf{X}_L^T}{\text{trace}\left(\mathbf{X}_L \mathbf{X}_L^T\right)} \quad \mathbf{R}_R = \frac{\mathbf{X}_R \mathbf{X}_R^T}{\text{trace}\left(\mathbf{X}_R \mathbf{X}_R^T\right)} \tag{8.8}$$

Then $\mathbf{R}_L$ and $\mathbf{R}_R$ are averaged across all trials, respectively, for left and right imagery cases, to get more robust estimates of the spatial covariance $\overline{\mathbf{R}_L}$ and $\overline{\mathbf{R}_R}$. The composite spatial covariance $\mathbf{R}$, as the sum of $\overline{\mathbf{R}_L}$ and $\overline{\mathbf{R}_R}$, can be diagonalized by singular value decomposition (SVD):

$$\mathbf{R} = \overline{\mathbf{R}_L} + \overline{\mathbf{R}_R} = \mathbf{U}_0 \Sigma \mathbf{U}_0^T \tag{8.9}$$

where $\mathbf{U}_0$ is the eigenvector matrix, and Σ is a diagonal matrix with corresponding eigenvalues as its diagonal elements. The variance in the space spanned by $\mathbf{U}_0$ components can be equalized by the following whitening matrix $\mathbf{P}$:

$$\mathbf{P} = \Sigma^{-1/2}\mathbf{U}_0^T \tag{8.10}$$

It can be shown that, if $\overline{\mathbf{R}_L}$ and $\overline{\mathbf{R}_R}$ are transformed into $\mathbf{S}_L$ and $\mathbf{S}_R$ by whitening matrix $\mathbf{P}$:

$$\mathbf{S}_L = \mathbf{P}\overline{\mathbf{R}_L}\mathbf{P}^T \quad \mathbf{S}_R = \mathbf{P}\overline{\mathbf{R}_R}\mathbf{P}^T \tag{8.11}$$

then $\mathbf{S}_L$ and $\mathbf{S}_R$ will share common eigenvalues. This means, given the SVD of $\mathbf{S}_L$ and $\mathbf{S}_R$,

$$\mathbf{S}_L = \mathbf{U}_L\Sigma_L\mathbf{U}_L^T \quad \mathbf{S}_R = \mathbf{U}_R\Sigma_R\mathbf{U}_R^T \tag{8.12}$$

the following equation holds true:

$$\mathbf{U}_L = \mathbf{U}_R = \mathbf{U} \quad \Sigma_L + \Sigma_R = \mathbf{I} \tag{8.13}$$

Thus, Σ_L and Σ_R may look like the following diagonal matrix:

$$\begin{aligned}\Sigma_L &= \mathrm{diag}\left[\overbrace{1\cdots1}^{m_L}\ \overbrace{\sigma_1\cdots\sigma_{m_C}}^{m_C}\ \overbrace{0\cdots0}^{m_R}\right]\\ \Sigma_R &= \mathrm{diag}\left[\overbrace{0\cdots0}^{m_L}\ \overbrace{\delta_1\cdots\delta_{m_C}}^{m_C}\ \overbrace{1\cdots1}^{m_R}\right]\end{aligned} \tag{8.14}$$

Because the sum of corresponding eigenvalues in Σ_L and Σ_R is always 1, the biggest eigenvalue of $\mathbf{S}_L$ corresponds to the smallest eigenvalue of $\mathbf{S}_R$. The eigenvectors in Σ_L corresponding to the first $\mathbf{m}$ eigenvalues in Σ_L are used to form a new transform matrix $\mathbf{U}_l$, which makes up the spatial filter with whitening matrix $\mathbf{P}$, for extracting the so-called *source activity* of left-hand imagery. The spatial filters for the left and the right cases are constructed as follows:

$$\mathbf{F}_L = \mathbf{U}_l^T\mathbf{P} \quad \mathbf{F}_R = \mathbf{U}_r^T\mathbf{P} \tag{8.15}$$

Then the source activities $\mathbf{Y}_L$ and $\mathbf{Y}_R$ are derived by applying the preceding spatial filter on bandpass-filtered EEG data matrix $\mathbf{X}$, that is,

$$\mathbf{Y}_L = \mathbf{F}_L \cdot \mathbf{X} \quad \mathbf{Y}_R = \mathbf{F}_R \cdot \mathbf{X} \tag{8.16}$$

Because of the way in which the spatial filter is derived, the filtered source activities $\mathbf{Y}_L$ and $\mathbf{Y}_R$ are expected to be better features for discriminating these two imagery tasks, compared with the original EEGs. Usually, the following inequation holds

true, which means the variance of the spatial filtered signal can be a good feature for classification purposes:

$$\text{var}(\mathbf{F}_L \cdot \mathbf{X}_L) > \text{var}(\mathbf{F}_R \cdot \mathbf{X}_L) \quad \text{var}(\mathbf{F}_R \cdot \mathbf{X}_R) > \text{var}(\mathbf{F}_L \cdot \mathbf{X}_R) \tag{8.17}$$

Alternatively, the band powers of $\mathbf{Y}_L$ and $\mathbf{Y}_R$ are more straightforward features. As shown in Figure 8.7, a more prominent peak difference can be seen on the power spectrum of the CSP-filtered signal than on the original power spectrum.

For the purpose of visualization, the columns of the inverse matrix of $\mathbf{F}_L$ and $\mathbf{F}_R$ can be mapped onto each EEG electrode to get a spatial pattern of CSP source distribution. As shown in the right-hand panel of Figure 8.7, the spatial distribution of $\mathbf{Y}_L$ and $\mathbf{Y}_R$ resembles the ERD topomap, which shows a clear focus in the left- and right-hand area over the sensorimotor cortex.

8.3.3 Online Three-Class SMR-Based BCI

8.3.3.1 BCI System Configuration

In this study, three states of motor imagery were employed to implement a multiclass BCI. Considering the reliable spatial distributions of ERD/ERS in sensorimotor cortex areas, imagination of body part movements including those of the left hand, right hand, and foot were considered as mental tasks for generating detectable brain patterns. We designed a straightforward online feedback paradigm, where real-time visual feedback was provided to indicate the control result of three

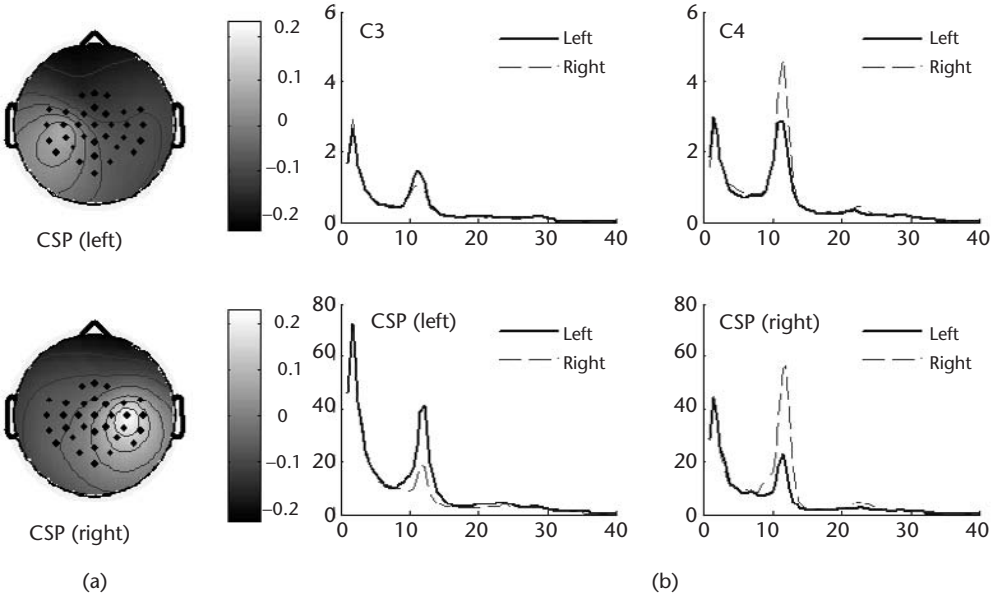

Figure 8.7 CSP spatial filtering enhances the SMR power difference between left- and right-hand motor imagery. (a) CSP spatial pattern of left- and right-hand imagery; and (b) the PSD of the temporal signal, with a solid line for left imagery and a dashed line for right imagery. Upper row: PSD of raw EEG from electrodes C3 and C4; lower row: PSD of derived CSP temporal signal.

directional movements, that is, left-hand, right-hand, and foot imagery for moving left, right, and forward, respectively.

Five right-handed volunteers (three males and two females, 22 to 27 years old) participated in the study. They were chosen from the subjects who could successfully perform two-class online BCI control in our previous study [55]. The recording was made using a BioSemi ActiveTwo EEG system. Thirty-two EEG channels were measured at positions involving the primary motor area (M1) and the supplementary motor area (SMA) (see Figure 8.8). Signals were sampled at 256 Hz and preprocessed by a 50-Hz notch filter to remove the power line interference, and a 4- to 35-Hz bandpass filter to retain the EEG activity in the mu and beta bands.

Here we propose a three-phase approach to allow for better adaptation between the brain and the computer algorithm. The detailed procedure is shown in Figure 8.9. For phase 1, a simple feature extraction and classification method was used for

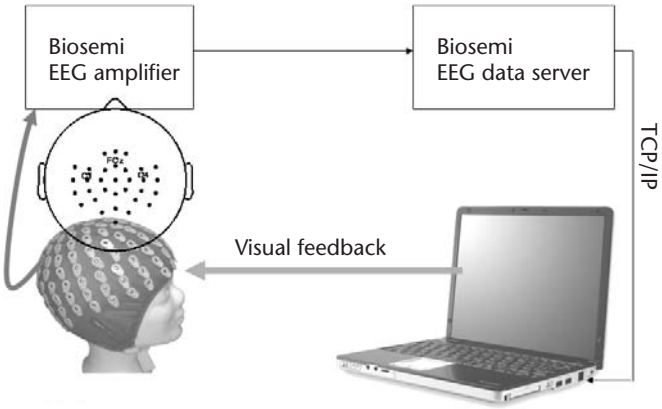

Figure 8.8 System configurations for an online BCI using the motor imagery paradigm. EEG signals were recorded with electrodes over sensorimotor and surrounding areas. The amplified and digitized EEGs were transmitted to a laptop computer, where the online BCI program translated it into screen cursor movements for providing visual feedback for the subject.

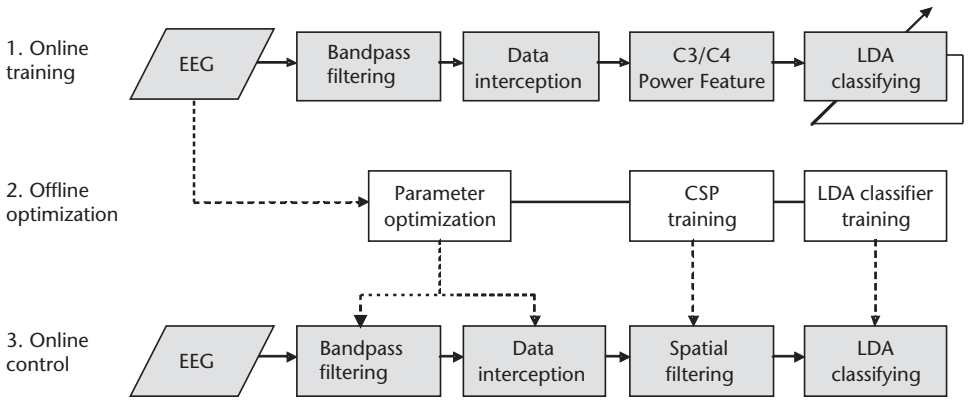

Figure 8.9 Flowchart of three-phase brain computer adaptation. The brain and BCI algorithm were first coadapted in an initial training phase, then the BCI algorithm was optimized in the following phase for better online control in the last phase.

online feedback training, allowing for the initial adaptation of both the human brain and the BCI algorithm. For phase 2, the recorded data from phase 1 were employed to optimize the feature extraction and to refine the classifier parameters for each individual, aiming at a better BCI algorithm through refined machine learning. For the real testing phase, phase 3, three-class online control was achieved by coupling the trained brain and optimized BCI algorithm.

8.3.3.2 Phase 1: Simple Classifier for Brain and Computer Online Adaptation

Figure 8.10 shows the paradigm of online BCI training with visual feedback. The "left hand," "right hand," and "foot" movement imaginings were designated to control three directional movements: left, right, and upward, respectively. The subject sat comfortably in an armchair, opposite a computer screen that displayed the visual feedback. The duration of each trial was 8 seconds. During the first 2 seconds, while the screen was blank, the subject was in relaxing state. At second 2, a visual cue (arrow) was presented on the screen, indicating the imagery task to be performed.

The arrow pointing left, right, and upward indicated the task of imagination of left-hand, right-hand, and foot movement, respectively. At second 3, three progress bars with different colors started to increase simultaneously from three different directions. The value of each bar was determined by the accumulated classification results from a linear discriminant analysis (LDA), and it was updated every 125 ms. For example, if the current classification result is "foot," then the "up" bar will increase one step and the values of the other two bars will be retained. At second 8, a true or false mark appeared to indicate the final result of the trial through calculating the maximum value of the three progress bars, and the subject was asked to relax and wait for the next task. The experiment consisted of two or four sessions and each session consisted of 90 trials (30 trials per class). The dataset comprising 360 or 180 trials (120 or 60 trials per class) was used for further offline analysis.

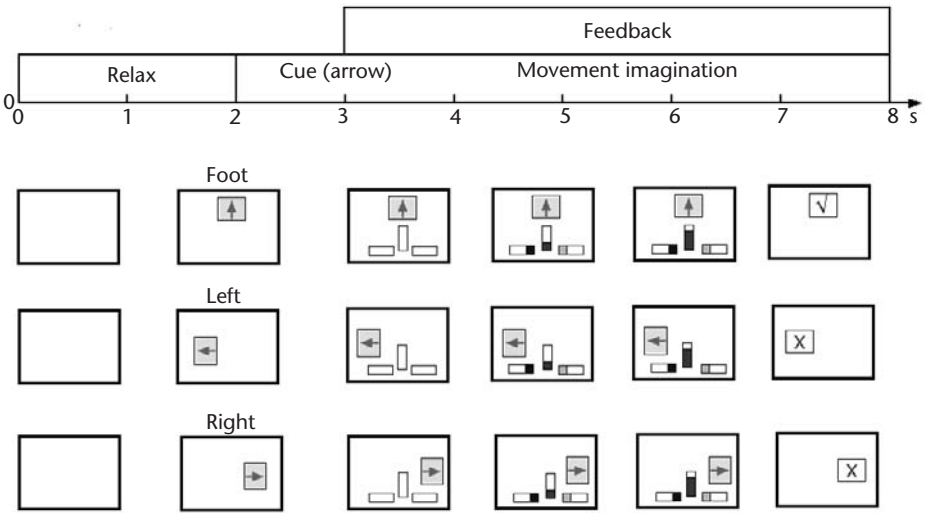

Figure 8.10 Paradigm of three-class online BCI training with visual feedback.

The features extracted for classification were bandpass power of mu rhythms on left and right primary motor areas (C3 and C4 electrodes). LDA was used to classify the bandpass power features on C3/C4 electrodes referenced to FCz [9]. A linear classifier was defined by a normal vector **w** and an offset **b** as

$$y = \text{sign}\left(\mathbf{w}^T \mathbf{x} + b\right) \tag{8.18}$$

where **x** was the feature vector. The values of **w** and **b** were determined by Fisher discriminant analysis (FDA). The three-class classification was solved by combining three binary LDA discriminant functions:

$$\begin{aligned} \mathbf{x}(t) &= \left[P_{C3}(t) P_{C4}(t)\right]^T \\ y_i(t) &= \text{sgn}\left(\mathbf{w}_i^T \mathbf{x}(t) + b_i\right), i = 1-3 \end{aligned} \tag{8.19}$$

where $P_{C3}(t)$ and $P_{C4}(t)$ are values of the average power in the nearest 1-second time window on C3 and C4, respectively. Each LDA was trained to discriminate two different motor imagery states. The decision rules are listed in Table 8.1, in which six combinations were designated to the three motor imagery states, respectively, with two combinations not classified.

An adaptive approach was used to update the LDA classifiers trial by trial. The initial normal vectors $\mathbf{w}_i^T$ of the classifiers were selected as [+1 –1], [0 –1], and [–1 0] (corresponding to the three LDA classifiers in Table 8.1) based on the ERD distributions. They were expected to recognize the imagery states through extracting the power changes of mu rhythms caused by contralateral distribution of ERD during left- and right-hand imagery, but bilateral power equilibrium during foot imagery over M1 areas [47, 48]. The initial **b** was set to zero.

When the number of samples reached five trials per class, the adaptive training began. Three LDA classifiers were updated trial by trial, gradually improving the generalization ability of the classifiers along with the increase of the training samples. This kind of gradual updating of classifiers provided a chance for initial user brain training and system calibration in an online BCI.

Figure 8.11 shows the probability that three progress bars won during an online feedback session. In each motor imagery task, the progress bar that has the maxi-

Table 8.1 Decision Rules for Classifying the Three Motor Imagery States Through Combining the Three LDA Classifiers

Left Versus Right	*Left Versus Foot*	*Right Versus Foot*	*Decision*
+1	+1	–1	Left
+1	+1	+1	Left
–1	+1	+1	Right
–1	–1	+1	Right
+1	–1	–1	Foot
–1	–1	–1	Foot
+1	–1	+1	None

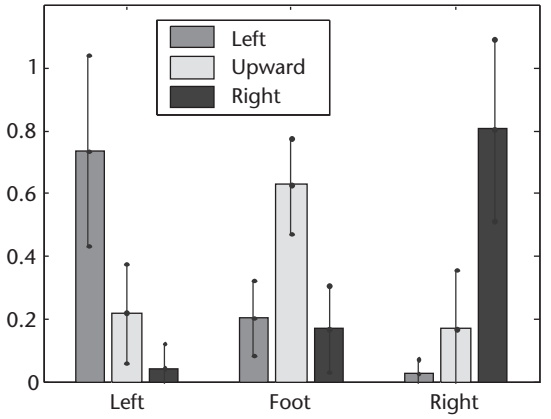

Figure 8.11 Winning probability of three progress bars in three-class motor imagery (one subject, 120 trials per class).

mum value correctly indicates the true label of the corresponding class. For example, during foot imagination, the "up" bar had a much higher value than the "left" and "right" bars; therefore, for most foot imagery tasks, the final decision was correct although some errors may occur.

8.3.3.3 Phase 2: Offline Optimization for Better Classifier

To improve the classification accuracy, we used the common spatial patterns method, as described earlier, to improve the SNR of the mu rhythm through extracting the task-related EEG components.

The CSP multiclass extensions have been considered in [56]. Three different CSP algorithms were presented based on one-versus-one, one-versus-rest, and approximate simultaneous diagonalization methods. Similar to the design of binary classifiers, the one-versus-one method was employed in our system to estimate the task-related source activities as the input of the binary LDA classifiers. It can be easily understood and with fewer unclassified samples compared to the one-versus-rest method. The design of spatial filters through approximate simultaneous diagonalization requires a large amount of calculation and the selection of the CSP patterns is more difficult than the two-class version.

As illustrated earlier in Figure 8.9, before online BCI control, the CSP-based training procedure was performed to determine the parameters for data preprocessing, the CSP spatial filters, and the LDA classifiers. A sliding window method was integrated to optimize the frequency band and the time window for data preprocessing in the procedure of joint feature extraction and classification. The accuracy was estimated by a 10×10-fold cross-validation. The optimized parameters, CSP filters, and LDA classifiers were used to implement the online BCI control and ensured a more robust performance compared with the online training procedure.

Table 8.2 lists the parameters for data preprocessing and the classification results for all subjects. The passband and the time window are subject-specific parameters that can significantly improve the classification performance. Average accuracy derived from online and offline analysis was 79.48% and 85.00%, respec-

Table 8.2 Classification Accuracies of Three Phases

Subjects	*Passband (Hz)*	*Time Window (seconds)*	*Phase 1 Accuracy (%)*	*Phase 2 Accuracy (%)*	*Phase 3 Accuracy (%)*
S1	10–35	2.5–8	94.00	98.11	97.03
S2	13–15	2.5–7.5	94.67	97.56	95.74
S3	9–15	2.5–7	74.71	80.13	81.32
S4	10–28	2.5–6	68.00	77.00	68.40
S5	10–15	2.5–7.5	66.00	72.22	71.50
Mean	—	—	79.48	85.00	82.80

tively. For subjects S1 and S2, no significant difference existed between the classification results of the three binary classifiers, and a high accuracy was obtained for three-class classification. For the other three subjects, the foot task was difficult to recognize, and the three-class accuracy was much lower than the accuracy of classifying left- and right-hand movements. This result may be caused by less training of the foot imagination, because all of the subjects did more training sessions of hand movement in previous studies of two-class motor imagery classification [55]. The average offline accuracy was about 5% higher than the online training phase due to the employment of parameter optimization and the CSP algorithm applied to multichannel EEG data.

8.3.3.4 Phase 3: Online Control of Three-Direction Movement

In phase 3, a similar online control paradigm as in phase 1 was first employed to test the effect of parameter optimization, and a 3% increase in online accuracy was observed. Then, three of the subjects participated in online control of three-direction movement of robot dogs (SONY, Aibo) for mimicking a brain signal controlled robo-cup game, in which one subject controlled the *goalkeeper* and the other controlled the *shooter*. This paradigm and approach could be used for applications such as wheelchair control [57] and virtual reality gaming [58, 59].

8.3.4 Alternative Approaches and Related Issues

8.3.4.1 Coadaptation in SMR-Based BCI

As discussed in Section 8.1.2, the BCI is not just a feedforward translation of brain signals into control commands; rather, it is about the bidirectional adaptation between the human brain and a computer algorithm [2, 6, 60], in which real-time feedback plays a crucial role during coadaptation.

For an SSVEP-based BCI system, the amplitude modulation of target EEG signals is automatically achieved by voluntary direction of the gaze direction and only the primary visual area is involved in the process. In contrast, for an SMR-based BCI system, the amplitude of the mu and/or beta rhythm is modulated by the subject's voluntary manipulation of his or her brain activity over the sensorimotor area, in which secondary, even high-level, brain areas are possibly involved. Thus, the

BCI paradigm with proper consideration of coadaptation feasibility is highly preferred for successful online BCI operation.

As summarized by McFarland et al. [61], there are at least three different paradigms for training (coadaptation) in an SMR-based BCI: (1) the "let the machines learn" approach, best demonstrated by the Berlin BCI group on naive subjects [51]; (2) the "let the brain learn" or "operant-conditioning," best demonstrated by the Tübingen BCI group on well-trained subjects [62]; or (3) the "let the brain and computer learn and coadapt simultaneously," best demonstrated by the Albany BCI group on well-trained subjects [12, 61]. Basically, the third approach fits the condition of online BCI control best, but poses the challenge of online algorithm updating, especially when a more complicated spatial filter is considered.

Alternatively, we have proposed a three-step BCI training paradigm for coadaptation. The brain was first trained for a major adaptation, then the BCI algorithm was trained offline, and finally the trained brain and fine-tuned BCI algorithm were coupled to provide better online operation. This can be best expressed by the statement "let the brain learn first, then the machines learn," which results in a compromise between maintaining an online condition and the more simple task of online algorithm updating.

8.3.4.2 Optimization of Electrode Placement

Different spatial distribution of SMR over sensorimotor areas is the key to discriminating among different imagery brain states. Although the topographic organization of the body map is genetic and conservative, each individual displays considerable variability because of the handiness, sports experience, and other factors that may cause a plastic change in the sensorimotor cortex. To deal with this spatial variability, a subject-specific spatial filter has proven to be very effective in the case of multiple-electrode EEG recordings. For a practical or portable BCI system, placing fewer EEG electrodes is preferred. Thus, it is crucial to determine the optimal electrode placement for capturing SMR activity effectively.

In a typical SMR-based BCI setting [48], six EEG electrodes were placed over the cortical hand areas: C3 for the right hand, C4 for the left hand, and two supplementary electrodes at positions anterior and posterior to C3/C4. Different bipolar settings, such as anterior-central (a-c), central-posterior (c-p), and anterior-posterior (a-p), were statistically compared and a-c bipolar placement was verified as the optimal one for capturing mu-rhythm features for 19 out of 34 subjects.

Instead of this typical setting, for considering the physiological role of the supplementary motor area (SMA), we proposed a novel electrode placement with only two bipolar electrode pairs: C3-FCz and C4-FCz. Functional neuroimaging studies indicated that motor imagery also activates the SMA [63] (roughly under electrode FCz). We investigated the phase synchronization of mu rhythms between the SMA and the hand area in M1 (roughly under electrode C3/C4) and observed a contralaterally increased synchronization similar to the ERD distribution [55]. This phenomenon makes it possible to utilize the signal over the SMA to enhance the significance of the power difference between M1 areas, by considering SMA (FCz) as the reference. It was demonstrated to be optimal for recognizing motor imagery states, which can satisfy the necessity of a practical BCI [64]. This simple and effec-

tive electrode placement can be a default setting for most subjects. For a more subject-specific optimization, ICA can be employed to find the "best" bipolar electrode pairs to retain the mu rhythm relevant signal components and to avoid other noisy components, which is similar with that described in the Section 8.2.2.3.

8.3.4.3 Visual Versus Kinesthetic Motor Imagery

As discussed in Section 8.1.2, an EEG-based BCI system requires the BCI user to generate specific EEG activity associated with the intent he or she wants to convey. The effectiveness of producing the specific EEG pattern by the BCI user largely determines the performance of the BCI system. In SMR-based BCI, for voluntary modulation of the μ or β rhythm, the BCI user needs to do movement imagination of body parts. Two types of mental practice of motor imagery are used: *visual* motor imagery, in which the subject produces a visual image (mental video) of body movements in the mind, and *kinesthetic* imagery, in which the subject rehearses his or her own action performed with imagined kinesthetic feelings.

In a careful comparison of these two categories of motor imagery, the kinesthetic method produced more significant SMR features than the visual one [65]. In our experience with SMR-based BCI, those subjects who get used to kinesthetic motor imagery perform better than those who do not. And usually, given same experiment instructions, most of the naïve subjects tend to choose visual motor imagery, whereas well-trained subjects prefer kinesthetic imagery. As shown in Neuper et al.'s study [65], the spatial distribution of SMR activity on the scalp varies between these two types of motor imagery, which implies the necessity for careful design of the spatial filter or electrode placement to deal with this spatial variability.

8.3.4.4 Phase Synchrony as BCI Features

Most BCI algorithms for classifying EEGs during motor imagery are based on the feature derived from power analysis of SMR. Phase synchrony as a bivariate EEG measurement could be a supplementary, even an independent, feature for novel BCI algorithms. Because phase synchrony is a bivariate measurement, it is subject to the proper selection of electrode pairs for the calculation. Basically, two different approaches are used. One is a random search among all possible electrode pairs with a criteria function related to the classification accuracy [66, 67]; the other is a semi-optimal approach that employs physiological prior knowledge to select the appropriate electrode pairs. Note that the latter approach has the advantage of lower computation costs, robustness, and better generalization ability, which has been shown in our study [55].

We noticed that phase coherence/coupling has been widely used in the physiology community and motor areas beyond primary sensorimotor cortex have been explored to find the neural coupling between these areas. Gerloff et al. demonstrated that, for both externally and internally paced finger extensions, functional coupling occurred between the primary sensorimotor cortex (SM1) of both hemispheres and between SM1 and the mesial premotor (PM) areas, probably including the SMA [68]. The study of event-related coherence showed that synchronization

between mu rhythms occurred in the precentral area and SM1 [69]. Spiegler et al. investigated phase coupling between different motor areas during tongue-movement imagery and found that phase-coupled 10-Hz oscillations were induced in SM1 and SMA [70]. All of this evidence points to the possible neural synchrony between SMA (and/or PM) and SM1 during the motor planning, as well as the motor imagery. Thus, we chose electrode pairs over SM1 and SMA as the candidate for phase synchrony measurement.

In one of our studies [55], a phase-locking value was employed to quantify the level of phase coupling during imagination of left- or right-hand movements, between SM1 and SMA electrodes. To the best of our knowledge, for the first time, use of a phase-locking value between the SM1 and SMA in the band of the mu rhythm was justified as additional features for the classification of left- or right-hand motor imagery, which contributed almost as much of the information as the power of the mu rhythm in the SM1 area. A similar result was also obtained by using a nonlinear regressive coefficient [71].

8.4 Concluding Remarks

8.4.1 BCI as a Modulation and Demodulation System

In this chapter, brain computer interfaces based on two types of oscillatory EEGs—the SSVEP from the visual cortex and the SMR from the motor cortex—were introduced and details of their physiological bases, example systems, and implementation approaches were given. Both of these BCI systems use oscillatory signals as the information carrier and, thus, can be thought of as modulation and demodulation systems, in which the human brain acts as a modulator to embed the BCI user's voluntary intent in the oscillatory EEG. The BCI algorithm then demodulates the embedded information into predefined codes for devices control.

In SSVEP-based BCI, the user modulates the photonic-driven response of the visual cortex by directing his or her gaze direction (or visual attention) to the target with different flashing frequencies. With an enhanced target frequency component, the BCI algorithm is able to use frequency detection to extract the predefined code, which largely resembles the process of frequency demodulation. Note that the carried information is a set of discrete BCI codes, instead of a continuous value, and the carrier signal here is much more complicated than a typical pure oscillation, covering a broad band of peri-alpha rhythms, along with other spontaneous EEG components. The SMR-based BCI system, however, resembles an amplitude modulation and demodulation system in which the BCI user modulates the amplitude of the mu rhythm over the sensorimotor cortex by doing specific motor imagery, and the demodulation is done by extracting the amplitude change of the mu-band EEG. The difference from typical amplitude modulation and demodulation systems is that two or more modulated EEG signals from specific locations are combined to derive a final code, for example, left, right, or forward.

For both of the BCI systems, the BCI code is embedded in an oscillatory signal, either as its amplitude or its frequency. As stated at the beginning of this chapter, this type of BCI bears the merit of robust signal transmission and easy signal processing. All examples demonstrated and reviewed in previous sections have indi-

cated a promising perspective for real applications. However, it cannot escape from the challenge of nonlinear and dynamic characteristics of brain systems as well, especially in terms of information modulation. The way in which the brain encodes/modulates the BCI code into the EEG activity varies across subjects and changes with time. These factors pose the challenge of coadaptation as discussed in the previous section. This suggests again that BCI system design is not just about the algorithm and that human factors should be considered very seriously.

8.4.2 System Design for Practical Applications

For the BCI systems discussed here, many studies have been done to implement and evaluate demonstration systems in the laboratory; however, the challenge facing the development of practical BCI systems for real-life application is still worth emphasizing. According to a survey done by Mason et al. [72], the existing BCI systems could be divided into three classes: transducers, demo systems, and assistive devices. Among the 79 BCI groups investigated, 10 have realized assistive devices (13%), 26 have designed demonstration systems (33%), and the remaining 43 are only in the stage of offline data analysis (54%). In other words, there is still a long way to go before BCI systems can be put into practical use. However, as an emerging engineering research field, if it can only stay in the laboratory for scientific exploration, its influence on human society will certainly be limited. Thus, the feasibility of creating practical applications is a serious challenge for BCI researchers. A practical BCI system must fully consider the user's human nature, which includes the following two key aspects:

1. *A better electrode system is needed that allows for convenient and comfortable use.* Current EEG systems use standard wet electrodes, in which electrolytic gel is required to reduce electrode-skin interface impedance. Using electrolytic gel is uncomfortable and inconvenient, especially if a large number of electrodes are adopted. First of all, preparations for EEG recording before BCI operation are time consuming. Second, problems caused by electrode damage or bad electrode contact can occur. Third, an electrode cap with large numbers of electrodes is uncomfortable for users to wear and then not suitable for long-term recording. Moreover, an EEG recording system with a high number of channels is usually quite expensive and not portable. For all of these reasons, reducing the number of electrodes in a BCI system is a critical issue and, currently, it has become the bottleneck in developing an applicable BCI system. In our system, we use a subject-specific electrode placement optimization method to achieve a high SNR for SSVEP and SMR. Although we demonstrated the applicability of the subject-specific positions in many online experiments, much work is still needed to explore the stationarity of the optimized electrode positions. Alternatively, more convenient electrode designs, for example, one that uses dry electrodes [44, 73], are highly preferable to replace the currently used wet electrode system.
2. *Better signal recording and processing is needed to allow for stable and reliable system performance.* Compared with the environment in an EEG

laboratory, electromagnetic interference and other artifacts (e.g., EMGs and EOGs) are much stronger in daily home life. Suitable measures then need to be applied to ensure the quality of the EEG recordings. Therefore, for data recording in an unshielded environment, the use of active electrodes may be better than the use of passive electrodes. Such usage can ensure that the recorded signal is less sensitive to interference. To remove the artifacts in EEG signals, additional recordings of EMGs and EOGs may be necessary and advanced techniques for online artifact canceling should be applied. Moreover, to reduce the dependence on technical assistance during system operation, ad hoc functions should be provided in the system to adapt to the individual diversity of the user and nonstationarity of the signal caused by changes of electrode impedance or brain state. These functions must be convenient for users to employ. For example, software should be able to detect bad electrode contacts in real time and adjust the algorithms to fit the remaining good channels automatically.

Acknowledgments

This work was partly supported by the National Natural Science Foundation of China (30630022, S. Gao, 60675029, B. Hong) and the Tsinghua-Yu-Yuan Medical Sciences Fund (B. Hong).

References

[1] Lebedev, M. A., and M. A. Nicolelis, "Brain-Machine Interfaces: Past, Present and Future," *Trends Neurosci.,* Vol. 29, No. 9, 2006, pp. 536–546.

[2] Wolpaw, J. R., et al., "Brain-Computer Interfaces for Communication and Control," *Clin. Neurophysiol.,* Vol. 113, No. 6, 2002, pp. 767–791.

[3] Schwartz, A. B., et al., "Brain-Controlled Interfaces: Movement Restoration with Neural Prosthetics," *Neuron,* Vol. 52, No. 1, 2006, pp. 205–220.

[4] Serruya, M. D., et al., "Instant Neural Control of a Movement Signal," *Nature,* Vol. 416, No. 6877, 2002, pp. 141–142.

[5] Wessberg, J., et al., "Real-Time Prediction of Hand Trajectory by Ensembles of Cortical Neurons in Primates," *Nature,* Vol. 408, No. 6810, 2000, pp. 361–365.

[6] Taylor, D. M., S. I. Tillery, and A. B. Schwartz, "Direct Cortical Control of 3D Neuroprosthetic Devices," *Science,* Vol. 296, No. 5574, 2002, pp. 1829–1832.

[7] Santhanam, G., et al., "A High-Performance Brain-Computer Interface," *Nature,* Vol. 442, No. 7099, 2006, pp. 195–198.

[8] Hochberg, L. R., et al., "Neuronal Ensemble Control of Prosthetic Devices by a Human with Tetraplegia," *Nature,* Vol. 442, No. 7099, 2006, pp. 164–171.

[9] Leuthardt, E. C., et al., "A Brain-Computer Interface Using Electrocorticographic Signals in Humans," *J. Neural Eng.,* Vol. 1, No. 2, 2004, pp. 63–71.

[10] Bashashati, A., et al., "A Survey of Signal Processing Algorithms in Brain-Computer Interfaces Based on Electrical Brain Signals," *J. Neural Eng.,* Vol. 4, No. 2, 2007, pp. R32–R57.

[11] Pfurtscheller, G., et al., "Mu Rhythm (De) Synchronization and EEG Single-Trial Classification of Different Motor Imagery Tasks," *NeuroImage,* Vol. 31, No. 1, 2006, pp. 153–159.

[12] Wolpaw, J. R., D. J. McFarland, and E. Bizzi, "Control of a Two-Dimensional Movement Signal by a Noninvasive Brain-Computer Interface in Humans," *Proc. Natl. Acad. Sci. USA,* Vol. 101, No. 51, 2004, pp. 17849–17854.

[13] Blankertz, B., et al., "The Berlin Brain-Computer Interface: EEG-Based Communication Without Subject Training," *IEEE Trans. on Neural Syst. Rehabil. Eng.,* Vol. 14, No. 2, 2006, pp. 147–152.

[14] Cheng, M., et al., "Design and Implementation of a Brain-Computer Interface with High Transfer Rates," *IEEE Trans. on Biomed. Eng.,* Vol. 49, No. 10, 2002, pp. 1181–1186.

[15] Middendorf, M., et al., "Brain-Computer Interfaces Based on the Steady-State Visual-Evoked Response," *IEEE Trans. on Rehabil. Eng.,* Vol. 8, No. 2, 2000, pp. 211–214.

[16] Birbaumer, N., et al., "A Spelling Device for the Paralysed," *Nature,* Vol. 398, No. 6725, 1999, pp. 297–298.

[17] Hinterberger, T., et al., "A Brain-Computer Interface (BCI) for the Locked-In: Comparison of Different EEG Classifications for the Thought Translation Device," *Clin. Neurophysiol.,* Vol. 114, No. 3, 2003, pp. 416–425.

[18] Donchin, E., K. M. Spencer, and R. Wijesinghe, "The Mental Prosthesis: Assessing the Speed of a P300-Based Brain-Computer Interface," *IEEE Trans. on Rehabil. Eng.,* Vol. 8, No. 2, 2000, pp. 174–179.

[19] Krusienski, D. J., et al., "Toward Enhanced P300 Speller Performance," *J. Neurosci. Methods,* Vol. 167, No. 1, 2008, pp. 15–21.

[20] Wolpaw, J. R., "Brain-Computer Interfaces as New Brain Output Pathways," *J. Physiol.,* Vol. 579, No. 3, 2007, p. 613.

[21] Blankertz, B., et al., "Optimizing Spatial Filters for Robust EEG Single-Trial Analysis," *IEEE Signal Processing Mag.,* Vol. 25, No. 1, 2008, pp. 41–56.

[22] Kachenoura, A., et al., "ICA: A Potential Tool for BCI Systems," *IEEE Signal Processing Mag.,* Vol. 25, No. 1, 2008, pp. 57–68.

[23] Lotte, F., et al., "A Review of Classification Algorithms for EEG-Based Brain-Computer Interfaces," *J. Neural Eng.,* Vol. 4, No. 2, 2007, pp. R1–R13.

[24] Pineda, J. A., et al., "Learning to Control Brain Rhythms: Making a Brain-Computer Interface Possible," *IEEE Trans. on Neural Syst. Rehabil. Eng.,* Vol. 11, No. 2, 2003, pp. 181–184.

[25] Regan, D., *Human Brain Electrophysiology: Evoked Potentials and Evoked Magnetic Fields in Science and Medicine,* New York: Elsevier, 1989.

[26] Hoffmann, U., et al., "An Efficient P300-Based Brain-Computer Interface for Disabled Subjects," *J. Neurosci. Methods,* Vol. 167, No. 1, 2008, pp. 115–125.

[27] Celesia, G. G., and N. S. Peachey, "Visual Evoked Potentials and Electroretinograms," in *Electroencephalography: Basic Principles, Clinical Applications, and Related Fields*, E. Niedermeyer and F. H. Lopes da Silva, (eds.), Baltimore, MD: Williams and Wilkins, 1999, pp. 1017–1043.

[28] Vidal, J. J., "Toward Direct Brain-Computer Communication," *Ann. Rev. Biophys. Bioeng.,* Vol. 2, 1973, pp. 157–180.

[29] Sutter, E. E., "The Brain Response Interface: Communication Through Visually Induced Electrical Brain Responses," *J. Microcomputer Applications,* Vol. 15, No. 1, 1992, pp. 31–45.

[30] Gao, X., et al., "A BCI-Based Environmental Controller for the Motion-Disabled," *IEEE Trans. on Neural Syst. Rehabil. Eng.,* Vol. 11, No. 2, 2003, pp. 137–140.

[31] Wang, Y., et al., "A Practical VEP-Based Brain-Computer Interface," *IEEE Trans. on Neural Syst. Rehabil. Eng.,* Vol. 14, No. 2, 2006, pp. 234–239.

[32] Muller-Putz, G. R., et al., "Steady-State Visual Evoked Potential (SSVEP)–Based Communication: Impact of Harmonic Frequency Components," *J. Neural Eng.,* Vol. 2, No. 4, 2005, pp. 123–130.

[33] Muller-Putz, G. R., et al., "Steady-State Somatosensory Evoked Potentials: Suitable Brain Signals for Brain-Computer Interfaces?" *IEEE Trans. Neural Syst. Rehabil. Eng.,* Vol. 14, No. 1, 2006, pp. 30–37.

[34] Kelly, S. P., et al., "Visual Spatial Attention Control in an Independent Brain-Computer Interface," *IEEE Trans. Biomed. Eng.,* Vol. 52, No. 9, 2005, pp. 1588–1596.

[35] Trejo, L. J., R. Rosipal, and B. Matthews, "Brain-Computer Interfaces for 1-D and 2-D Cursor Control: Designs Using Volitional Control of the EEG Spectrum or Steady-State Visual Evoked Potentials," *IEEE Trans. on Neural Syst. Rehabil. Eng.,* Vol. 14, No. 2, 2006, pp. 225–229.

[36] Wang, Y., et al., "Lead Selection for SSVEP-Based Brain-Computer Interface," *Proc. IEEE Engineering in Medicine and Biology Society Conf.,* Vol. 6, 2004, pp. 4507–4510.

[37] Kluge, T., and M. Hartmann, "Phase Coherent Detection of Steady-State Evoked Potentials: Experimental Results and Application to Brain-Computer Interfaces," *3rd Int. IEEE/EMBS Conf. on Neural Engineering, CNE '07,* 2007, pp. 425–429.

[38] Vidal, J. J., "Real-Time Detection of Brain Events in EEG," *Proc. IEEE,* Vol. 65, No. 5, 1977, pp. 633–641.

[39] Lee, P. L., et al., "The Brain-Computer Interface Using Flash Visual Evoked Potential and Independent Component Analysis," *Ann. Biomed. Eng.,* Vol. 34, No. 10, 2006, pp. 1641–1654.

[40] Allison, B. Z., et al., "Towards an Independent Brain-Computer Interface Using Steady State Visual Evoked Potentials," *Clin. Neurophysiol.,* Vol. 119, No. 2, 2008, pp. 399–408.

[41] Morgan, S. T., J. C. Hansen, and S. A. Hillyard, "Selective Attention to Stimulus Location Modulates the Steady-State Visual Evoked Potential," *Proc. Natl. Acad. Sci. USA,* Vol. 93, No. 10, 1996, pp. 4770–4774.

[42] Ding, J., G. Sperling, and R. Srinivasan, "Attentional Modulation of SSVEP Power Depends on the Network Tagged by the Flicker Frequency," *Cereb. Cortex,* Vol. 16, No. 7, 2006, pp. 1016–1029.

[43] Kelly, S. P., et al., "Visual Spatial Attention Tracking Using High-Density SSVEP Data for Independent Brain-Computer Communication," *IEEE Trans. on Neural Syst. Rehabil. Eng.,* Vol. 13, No. 2, 2005, pp. 172–178.

[44] Fonseca, C., et al., "A Novel Dry Active Electrode for EEG Recording," *IEEE Trans. on Biomed. Eng.,* Vol. 54, No. 1, 2007, p. 163.

[45] Friman, O., I. Volosyak, and A. Graser, "Multiple Channel Detection of Steady-State Visual Evoked Potentials for Brain-Computer Interfaces," *IEEE Trans. on Biomed. Eng.,* Vol. 54, No. 4, 2007, pp. 742–750.

[46] Lin, Z., et al., "Frequency Recognition Based on Canonical Correlation Analysis for SSVEP-Based BCIs," *IEEE Trans. on Biomed. Eng.,* Vol. 53, No. 12, Pt. 2, 2006, pp. 2610–2614.

[47] Pfurtscheller, G., and C. Neuper, "Motor Imagery and Direct Brain-Computer Communication," *Proc. IEEE,* Vol. 89, No. 7, 2001, pp. 1123–1134.

[48] Neuper, C., "Motor Imagery and EEG-Based Control of Spelling Devices and Neuroprostheses," in *Event-Related Dynamics of Brain Oscillations,* C. Neuper and W. Klimesch, (eds.), New York: Elsevier, 2006.

[49] MacKay, W. A., "Wheels of Motion: Oscillatory Potentials in the Motor Cortex," in *Motor Cortex in Voluntary Movements: A Distributed System for Distributed Functions*, *Methods, and New Frontiers in Neuroscience,* E. Vaadia and A. Riehle, (eds.), Boca Raton, FL: CRC Press, 2005, pp. 181–212.

[50] Pfurtscheller, G., and A. Aranibar, "Event-Related Cortical Desynchronization Detected by Power Measurements of Scalp EEG," *Electroencephalogr. Clin. Neurophysiol.,* Vol. 42, No. 6, 1977, pp. 817–826.

[51] Blankertz, B., et al., "The Noninvasive Berlin Brain-Computer Interface: Fast Acquisition of Effective Performance in Untrained Subjects," *NeuroImage,* Vol. 37, No. 2, 2007, pp. 539–550.

[52] Ramoser, H., J. Muller-Gerking, and G. Pfurtscheller, "Optimal Spatial Filtering of Single-Trial EEG During Imagined Hand Movement," *IEEE Trans. on Rehabil. Eng.,* Vol. 8, No. 4, 2000, pp. 441–446.

[53] McFarland, D. J., et al., "Spatial Filter Selection for EEG-Based Communication," *Electroencephalogr. Clin. Neurophysiol.,* Vol. 103, No. 3, 1997, pp. 386–394.

[54] Blankertz, B., et al., "Boosting Bit Rates and Error Detection for the Classification of Fast-Paced Motor Commands Based on Single-Trial EEG Analysis," *IEEE Trans. on Neural Syst. Rehabil. Eng.,* Vol. 11, No. 2, 2003, pp. 127–131.

[55] Wang, Y., et al., "Phase Synchrony Measurement in Motor Cortex for Classifying Single-Trial EEG During Motor Imagery," *Proc. IEEE Engineering in Medicine and Biology Society Conf.,* Vol. 1, 2006, pp. 75–78.

[56] Dornhege, G., et al., "Boosting Bit Rates in Noninvasive EEG Single-Trial Classifications by Feature Combination and Multiclass Paradigms," *IEEE Trans. on Biomed. Eng.,* Vol. 51, No. 6, 2004, pp. 993–1002.

[57] Tanaka, K., K. Matsunaga, and H. O. Wang, "Electroencephalogram-Based Control of an Electric Wheelchair," *IEEE Trans. on Robotics,* Vol. 21, No. 4, 2005, pp. 762–766.

[58] Bayliss, J. D., and D. H. Ballard, "A Virtual Reality Testbed for Brain-Computer Interface Research," *IEEE Trans. on Rehabil. Eng.,* Vol. 8, No. 2, 2000, pp. 188–190.

[59] Pfurtscheller, G., et al., "Walking from Thought," *Brain Res.,* Vol. 1071, No. 1, 2006, pp. 145–152.

[60] Shenoy, P., et al., "Towards Adaptive Classification for BCI," *J. Neural Eng.,* Vol. 3, No. 1, 2006, pp. R13–R23.

[61] McFarland, D. J., D. J. Krusienski, and J. R. Wolpaw, "Brain-Computer Interface Signal Processing at the Wadsworth Center: Mu and Sensorimotor Beta Rhythms," *Prog. Brain Res.,* Vol. 159, 2006, pp. 411–419.

[62] Birbaumer, N., et al., "The Thought-Translation Device (TTD): Neurobehavioral Mechanisms and Clinical Outcome," *IEEE Trans. on Neural Syst. Rehabil. Eng.,* Vol. 11, No. 2, 2003, pp. 120–123.

[63] Deiber, M. P., et al., "Cerebral Processes Related to Visuomotor Imagery and Generation of Simple Finger Movements Studied with Positron Emission Tomography," *NeuroImage,* Vol. 7, No. 2, 1998, pp. 73–85.

[64] Wang, Y., et al., "Design of Electrode Layout for Motor Imagery Based Brain-Computer Interface," *Electron Lett.,* Vol. 43, No. 10, 2007, pp. 557–558.

[65] Neuper, C., et al., "Imagery of Motor Actions: Differential Effects of Kinesthetic and Visual-Motor Mode of Imagery in Single-Trial EEG," *Cog. Brain Res.,* Vol. 25, No. 3, 2005, pp. 668–677.

[66] Gysels, E., and P. Celka, "Phase Synchronization for the Recognition of Mental Tasks in a Brain-Computer Interface," *IEEE Trans. Neural Syst. Rehabil. Eng.,* Vol. 12, No. 4, 2004, pp. 406–415.

[67] Brunner, C., et al., "Online Control of a Brain-Computer Interface Using Phase Synchronization," *IEEE Trans. on Biomed. Eng.,* Vol. 53, No. 12 Pt. 1, 2006, pp. 2501–2506.

[68] Gerloff, C., et al., "Functional Coupling and Regional Activation of Human Cortical Motor Areas During Simple, Internally Paced and Externally Paced Finger Movements," *Brain,* Vol. 121, 1998, pp. 1513–1531.

[69] Pfurtscheller, G., and C. Andrew, "Event-Related Changes of Band Power and Coherence: Methodology and Interpretation," *J. Clin. Neurophysiol.,* Vol. 16, No. 6, 1999, pp. 512–519.

[70] Spiegler, A., B. Graimann, and G. Pfurtscheller, "Phase Coupling Between Different Motor Areas During Tongue-Movement Imagery," *Neurosci. Lett.,* Vol. 369, No. 1, 2004, pp. 50–54.

[71] Wei, Q., et al., "Amplitude and Phase Coupling Measures for Feature Extraction in an EEG-Based Brain-Computer Interface," *J. Neural Eng.,* Vol. 4, No. 2, 2007, pp. 120–129.

[72] Mason, S. G., et al., "A Comprehensive Survey of Brain Interface Technology Designs," *Ann. Biomed. Eng.,* Vol. 35, No. 2, 2007, pp. 137–169.

[73] Popescu, F., et al., "Single-Trial Classification of Motor Imagination Using 6 Dry EEG Electrodes," *PLoS ONE,* Vol. 2, No. 7, 2007, p. e637.